

Design of Two-Phase DC-AC Interleaved Boost Inverter with Voltage Control System using PI Controller

Juan M. A. Wasiatno*, Leonardus H. Pratomo

*Department of Electrical Engineering
Soegijapranata Catholic University
Jl. Pawiyatan Luhur Sel. IV No.1, Bendan Duwur, Gajahmungkur
Semarang, Indonesia*

Abstract

DC-DC Interleaved Boost Converter (DC-DC IBC) topology was developed through the interleaving technique since conventional DC-DC Boost Converter has many problems related to complex circuit control, harmonics, and output power. In this research, DC-DC IBC was developed into a Two-Phase AC-AC Interleaved Boost Converter (TP AC-AC IBC), then combined with a Two-Phase Full Bridge Inverter to become a Two-Phase DC-AC Interleaved Boost Inverter (TP DC-AC IBI). TP DC-AC IBI has several advantages, including minimal current and voltage ripples and greater output power because it consists of two AC-AC IBCs. This research aims to meet highly regulated AC voltage needs with the renewable energy source input using the proposed topology, by implementing Proportional Integral (PI) close loop control system. The output voltage is detected using a voltage transducer LV-25P, then compared with a reference voltage and controlled using a PI controller to keep the output voltage consistently stable. The switching signal setting uses the Sinusoidal Pulse Width Modulation (SPWM) technique by modulating the control output with a high frequency. As a verification step, testing was carried out using Power Simulator (PSIM) software and then validated by hardware testing in the laboratory. Testing was carried out using several test signals, and it was found that the proposed method worked well. System efficiency and Total Harmonic Distortion (THD) tests carried out using various load values, and a maximum efficiency of 93.87% and a minimum THD of 2.46% were obtained.

Keywords: DC-AC interleaved boost inverter, full-bridge inverter, PI Controller, voltage control

I. INTRODUCTION

Renewable Energy (RE) trends are overgrowing these days due to global warming. RE sources, such as wind turbines and photovoltaic (PV) panels, as the provider of controlled output voltage in off-grid systems, it usually consists of two converters, namely the DC-DC Boost Converter (DC-DC BC) as a voltage increaser and an inverter as a DC/AC voltage converter. However, DC-DC BC has several performance constraints in the form of high output voltage and input current ripples, relatively small gain, and poor efficiency [1], [2]. As a solution, the interleaving or multi-phasing method is applied to BC [2], [3]. Interleaving in BC combines at least two BCs in parallel [1]-[3], resulting in a topology called a Two-Phase DC-DC Interleaved Boost Converter (TP DC-DC IBC). Each IBC's control operates with a 180° phase angle shift, as applied in research [4] and [5].

TP DC-DC IBC has several performance advantages compared to conventional BC, including minimal current and voltage ripples, higher voltage gain, higher energy density levels, and much better efficiency [1], [2], [6], [7]. Research [6] shows that IBC can produce efficiency of up to 95%. Ripple reduction also reduces voltage stress on the components [4], [7], [8]. Because of these advantages, TP DC-DC IBC is

popularly applied to meet high voltage needs in RE systems such as PV [7]-[9] and vehicle fuel cell systems [10], [11].

Electrical energy is mostly needed in AC, while the voltage output from RE sources is DC [12], [13]. Inverter must be used to convert DC into AC at certain frequency and voltage levels [14], [15]. The higher output voltage of the RE systems results in broader applications. Combining the Inverter with the BC circuit allows the system to generate higher AC voltage [12], [13].

Several studies have been carried out regarding DC/AC Conversion System. In [12], [16], [17], the DC-DC BC is used to increase the initial DC voltage from PV output before being converted into AC voltage using Inverter. In [11], [18], and [19], they used Three-Phase DC-DC IBC instead of DC-DC BC, while the Four-Phase type has been used in [20]. All those studies applied the same conventional Boost DC/AC Inverter topology structure, which has major disadvantages such as poor filter performances and relatively high voltage stress that will affect the system output's quality. A new, enhanced DC/AC Boost Inverter method is proposed. TP DC-DC IBC will be developed into a Two-Phase AC-AC Interleaved Boost Converter (TP AC-AC IBC) by adding several power switches arranged back and forth so that the IBC can work with AC input. TP DC-AC IBC's input side is then combined with the output from the Two-Phase Full Bridge Inverter (TP FBI), thus forming a new power circuit topology called a Two-Phase DC-AC Interleaved Boost Inverter (TP DC-AC IBI). The DC voltage from the input will be directly

* Corresponding Author.

Email: j.marc.alx030@gmail.com

Received: June 28, 2024 ; Revised: August 25, 2024

Accepted: September 4, 2024 ; Published: December 31, 2024

converted into AC with TP FBI and then boosted with TP AC-AC IBC. Although the proposed method will increase switching losses, it can further reduce the voltage stress of the electronic components, including the power switches on the TP AC-AC IBC, which will extend its service life. Moreover, the inductors on the circuit will not easily get saturated because they are working on AC. Thus, it increases the system's efficiency and reduces the current and voltage harmonics. Both advantages will further enhance the system's output signal quality.

Controlling the output voltage, especially in high-voltage applications, is essential [21]. According to [22] and [23], changes in output load can affect the system's stability. A closed loop system with Proportional Integral (PI) control is used to control and regulate the output voltage [22], [24], [25]. This research aims to meet highly regulated AC voltage needs with the RE source as the system's input using TP DC-AC IBI topology by applying the PI closed-loop control system for AC load usage. The PI controller will stabilize (regulate) the output voltage according to the reference voltage. The power circuit's output voltage is detected using a Voltage Transducer LV-25P, then compared with the reference value and, controlled with a PI controller, then modulated as a signal controller for each power switch (MOSFETs). The switching signal setting uses the Sinusoidal Pulse Width Modulation (SPWM) technique by modulating the control output with a high frequency. STM32F407VET6 microcontroller is used in this research, regulating the PI control algorithm and switching logic.

The explanation of how TP DC-AC IBI works and the proposed voltage control strategy are described in Section II. Section III will present the results of simulation and hardware testing then compare the two, as well as THD and efficiency testing. The conclusion of this research will be presented in Section IV.

II. METHODS

A. Two Phase DC-AC Interleaved Boost Inverter

Figure 1 is a schematic of the TP DC-AC IBC circuit, consisting of DC voltage source (V_{in}) considered as the RE DC Output, TP FBI and TP AC-AC IBC.

The TP FBI applied in this research is a two-phase, three-leg Voltage Source Inverter (VSI) with a Unipolar Pulse Width Modulation (Unipolar PWM) control method. It consists of six power switches, S1 – S6, which regulate the current path from the source to the

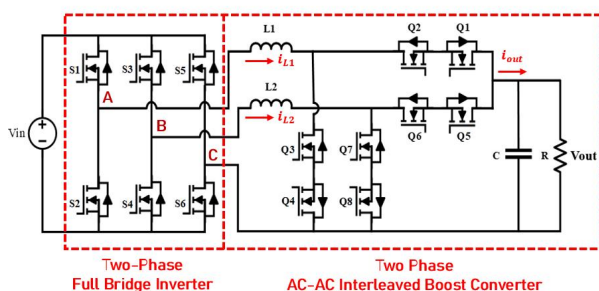


Figure 1 . Two Phase DC-AC IBI Schematic Diagram

power circuit and vice versa. A high-frequency SPWM switching technique is applied for S1 and S2 to regulate the current through Leg A. It is similar to S3 and S4 but for Leg B. Meanwhile, a low-frequency PWM switching technique is applied for S5 and S6 to regulate the current through Leg C as a Zero Crossing Detector (ZCD). Control signals for Leg A and Leg B are phase-shifted by 180° . Equation (1) shows the relation between the output voltage of TP FBI (V_{o_inv}) and V_{in}

$$V_{o_inv} = mV_{in} \quad (1)$$

where m is the Inverter's Modulation Index.

The output from the TP FBI will be connected to the TP AC-AC IBC circuit, which consists of two Inductors L1 and L2, six power switches Q1 – Q8, capacitor C and resistive load R. Inverter Leg A is connected to L1, Q1, Q2, Q3 and Q4 (the first AC-AC IBC), while Inverter Leg B is connected to L2, Q5, Q6, Q7 and Q8 (the second AC-AC IBC). A high-frequency PWM switching technique is applied for Q1 – Q8. Q1, Q4, Q5 and Q8 are placed in reverse as current paths in the negative cycle. Equation (2) shows the relation between the TP AC-AC IBC output voltage (V_o) to V_{o_inv}

$$V_o = \frac{V_{o_inv}}{1-D} \quad (2)$$

where D is the duty cycle of the control signals. Substitute (1) into (2), then the AC output voltage of TP DC-AC IBI (V_{out}) can be obtained using Equation (3).

$$V_{out} = V_o = \frac{mV_{in}}{1-D} \quad (3)$$

This research attempts V_{out} to become two times the V_{in} , so m was set at 1, while D was set at 50%.

B. Operational Modes

TP DC-AC IBI has four switching modes, which is a combination of the power switches conduction state (ON State) and non-conduction state (OFF State) in positive and negative cycles, with the flow as described in several studies [1], [3]-[5]. Table 1 shows the TP FBI switching pattern, while Table 2 shows the TP AC-AC IBC switching pattern, both on positive cycles.

Next is the explanation of each mode in the positive cycle referring to Figure 1, Table 1 and Table 2. In each mode, the voltage on L1 (V_{L1}), L2 (V_{L2}), and V_{out}

TABLE 1
TP FBI SWITCHING PATTERN ON POSITIVE CYCLE

Mode	S1	S2	S3	S4	S5	S6
1	On	Off	On	Off	Off	On
2	On	Off	On	Off	Off	On
3	On	Off	On	Off	Off	On
4	On	Off	On	Off	Off	On

TABLE 2
TP AC-AC IBC SWITCHING PATTERN ON POSITIVE CYCLE

Mode	Q1	Q2	Q3	Q4	Q5	Q6	Q7	Q8
1	Off	On	On	On	Off	On	On	On
2	On	On	Off	On	Off	On	On	On
3	Off	On	On	On	On	On	Off	On
4	On	On	Off	On	On	On	Off	On

will also be determined using KVL analysis [3], [4].

In the positive cycle, S1 and S3 are active using a 10 kHz SPWM switching technique, S6 is active using a 50 Hz PWM switching technique, while Q1, Q3, Q5, and Q7 are active with a 10 kHz PWM switching technique. Q2, Q4, Q6 and Q8 are always active, while S2, S4 and S5 are inactive.

1) In Mode 1, Q3 and Q7 are active. Current from DC Source (i_{in}) flows through S1 and S3, then charges energy in L1 and L2 so that the L1 current (i_{L1}) and L2 current (i_{L2}) increases. Next, i_{L1} flows back to inverter through Q3 and Q4, while i_{L2} through Q7 and Q8. Both currents flow back to V_{in} through S6. Simultaneously, the energy stored in C is released towards R (freewheeling).

Figure 2 is the equivalent TP DC-AC IBI circuit in Mode 1. V_{L1} , V_{L2} , and V_{out} formulas in this mode are shown in Equations (4a) – (4c).

$$V_{L1} = L1 \frac{di_{L1}}{dt} = V_{in} \quad (4a)$$

$$V_{L2} = L2 \frac{di_{L2}}{dt} = V_{in} \quad (4b)$$

$$V_{out} = V_C \quad (4c)$$

2) In Mode 2, Q7 is active, while Q3 is inactive. i_{in} flows through S3, then charges energy at L2 so i_{L2} increases. i_{L2} returns to V_{in} through Q7, Q8, and S6. Because Q3 is inactive, i_{L1} flows to C and R first through Q1 and Q2 before returning to V_{in} through S6. The energy stored in L1 is also discharged towards C and R so that i_{L1} decreases.

Figure 3 is the equivalent TP DC-AC IBI circuit in Mode 2. V_{L1} , V_{L2} , and V_{out} formulas in this mode are shown in Equations (5a) – (5c).

$$V_{L1} = L1 \frac{di_{L1}}{dt} = V_{out} - V_{in} \quad (5a)$$

$$V_{L2} = L2 \frac{di_{L2}}{dt} = V_{in} \quad (5b)$$

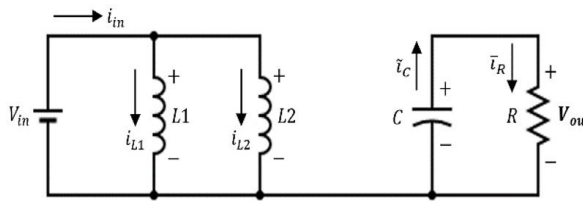


Figure 2. TP DC-AC IBI Equivalent Circuit in Mode 1

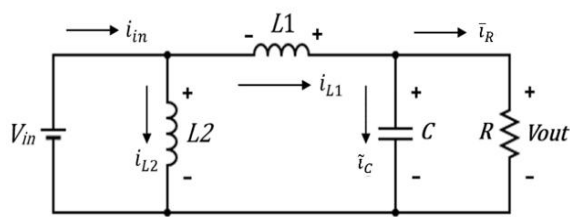


Figure 3. TP DC-AC IBI Equivalent Circuit in Mode 2

$$V_{out} = V_{in} + V_{L1} \quad (5c)$$

3) In Mode 3, Q3 is active, while Q7 is inactive. i_{in} flows through S1, then charges energy at L1 so i_{L1} increases. i_{L1} returns to V_{in} through Q3, Q4, and S6. Because Q7 is inactive, i_{L2} flows to C and R first through Q5 and Q6 before returning to V_{in} through S6. The energy stored in L2 is also discharged towards C and R so that i_{L2} decreases.

Figure 4 is the equivalent TP DC-AC IBI circuit in Mode 3. V_{L1} , V_{L2} and V_{out} formulas in this mode are shown in Equations (6a) – (6c).

$$V_{L1} = L1 \frac{di_{L1}}{dt} = V_{in} \quad (6a)$$

$$V_{L2} = L2 \frac{di_{L2}}{dt} = V_{out} - V_{in} \quad (6b)$$

$$V_{out} = V_{in} + V_{L2} \quad (6c)$$

4) In Mode 4, Q3 and Q7 are inactive. i_{in} flows through S1 and S3, then proceed towards C and R through Q1, Q2, Q5, and Q6. The energy stored in L1 and L2 are also discharged towards C and R so that i_{L1} and i_{L2} decreases. The currents return back to V_{in} through S6.

Figure 5 is the equivalent TP DC-AC IBI circuit in Mode 4. V_{L1} , V_{L2} and V_{out} formulas in this mode are shown in Equations (7a) – (7c).

$$V_{L1} = L1 \frac{di_{L1}}{dt} = V_{out} - V_{in} \quad (7a)$$

$$V_{L2} = L2 \frac{di_{L2}}{dt} = V_{out} - V_{in} \quad (7b)$$

$$V_{out} = V_{in} + V_{L1} = V_{in} + V_{L2} \quad (7c)$$

For the negative cycle (still referring to Figure 1), S2 and S4 are active using the 10 kHz SPWM switching technique, S6 is active using the 50 Hz PWM switching technique, while Q2 Q4, Q6 and Q8 are active with the

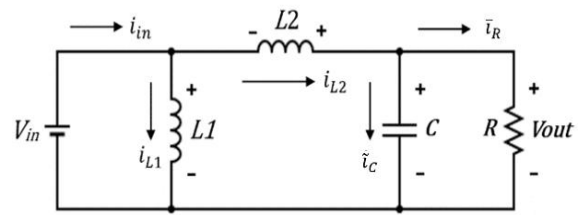


Figure 4. TP DC-AC IBI Equivalent Circuit in Mode 3

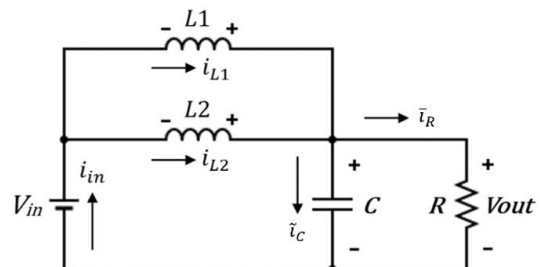


Figure 5. TP DC-AC IBI Equivalent Circuit in Mode 4

10 kHz PWM switching technique. Q1, Q3, Q5 and Q7 are always active, while S1, S3 and S6 are inactive.

Table 3 shows the TP FBI switching pattern, while Table 4 shows the TP AC-AC IBC switching pattern, both on negative cycle.

From Equations (5c), (6c) and (7c), it is known that V_{out} will always be greater than V_{in} . This theoretically proves the basic principle of the TP DC-AC IBC in this research as a voltage increaser. Figure 1 shows that the circuit output current (i_{out}) on average is the sum of the output currents from each IBC, which is shown in Equation (8) below.

$$i_{L1} + i_{L2} = i_{out} = \tilde{i}_C + \tilde{i}_R \quad (8)$$

Thus, the amount of power that can be generated on the output side of the TP DC-AC IBC (P_{out}) can be determined using Equation (9) below.

$$P_{out} = i_{out}V_{out} = (i_{L1} + i_{L2})V_{out} \quad (9)$$

From Equation (9) it is known that this topology can produce power up to twice the conventional BC.

C. Voltage Transducer LV-25P

This research uses a *Voltage Transducer* LV25-P as the sensor for V_{out} . The LV25-P output is the actual system value (V_{act}) which is then scaled to the maximum ADC value of the microcontroller (V_{ADC}) to carry out AC sampling voltage (STM32F407VET6 is used on this research). LV25-P was also used in [21] and [26] because of several advantages such as high reading accuracy, wide internal bandwidth, good linearization process, and better immunity to external interference.

Figure 6 is a circuit diagram of the LV-25P based on the datasheet. There are two terminals on the primary side, connected to V_{out} , namely '+ HT' and '-HT'. On the secondary side, there are three terminals. Terminal '+' and '-' are the power supply terminals (12 V – 15 V), while terminal 'M' or 'Measure' is the LV-25P output terminal, resulting V_{act} .

Based on the datasheet, it is known that the nominal primary r.m.s current (I_{in}) is 10 mA. The LV-25P can also read input voltage between 10 V – 500 V. V_{out} is adjusted to 100 VAC, so it is measurable for LV-25P.

TABLE 3
TP FBI SWITCHING PATTERN ON NEGATIVE CYCLE

Mode	S1	S2	S3	S4	S5	S6
1	Off	On	Off	On	On	Off
2	Off	On	Off	On	On	Off
3	Off	On	Off	On	On	Off
4	Off	On	Off	On	On	Off

TABLE 4
TP AC-AC IBC SWITCHING PATTERN ON NEGATIVE CYCLE

Mode	Q1	Q2	Q3	Q4	Q5	Q6	Q7	Q8
1	On	Off	On	On	On	Off	On	On
2	On	On	On	Off	On	Off	On	On
3	On	Off	On	On	On	On	On	Off
4	On	On	On	Off	On	On	On	Off

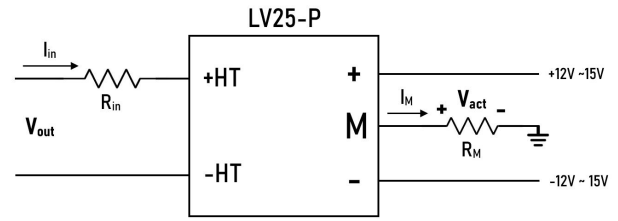


Figure 6. LV-25P Schematic Diagram

Applying Ohm's Law to achieve the I_{in} of 10mA, the LV-25P's input resistor (R_{in}) can be determined using Equation (10) below [21], [26]. Thus, a 10 k Ω 3 W resistor is used as R_{in} .

$$R_{in} \geq \frac{V_{out}}{I_{in}} = \frac{100V}{10mA} = 10k\Omega \quad (10)$$

There is also a measurement resistor R_M connected in series with the 'M' terminal, which value adjusting the V_{ADC} that is 3.3 V at maximum. Based on the datasheet, it is also known that the LV-25P has a Conversion Ratio 2500:1000, which is the nominal ratio of the secondary r.m.s current (I_M) to I_{in} . So, if I_{in} is 10 mA, then I_M is 25 mA. Therefore, for V_{ADC} 3.3 V, the value of R_M can be determined using Equation (11) below [21], [26]. Thus, a 150 Ω 0.5 W resistor is used as R_M .

$$R_M \geq \frac{V_{ADC}}{I_M} = \frac{3.3V}{25mA} = 132\Omega \quad (11)$$

D. PI Control

This research applies a close loop system as voltage control using Proportional Integral (PI) control as implemented in [22] and [25]. Figure 7 is a block diagram of PI control system in general.

PI control is a combination of Proportional and Integral control. Apart from being easy to implement, this control has a fast response time and minimum noise, thus chosen as a solution to overcome the output instability from TP DC-AC IBC due to load changes [22], [23], [25]. Referring to Figure 7, the PI control equation can be written in Equation (12) below [23], [24].

$$m(t) = K_p e(t) + K_i \int_0^t e(t) dt \quad (12)$$

K_p is the Proportional Gain, K_i is the Integral Gain, and $m(t)$ is the actual output of the system, which is V_{act} in this research. K_p and K_i values are obtained by trial-and-error method until an appropriate value is found. $e(t)$ is the system error, the difference between the desired or reference value $r(t)$ and $m(t)$, which is formulated in Equation (13) [23], [24].

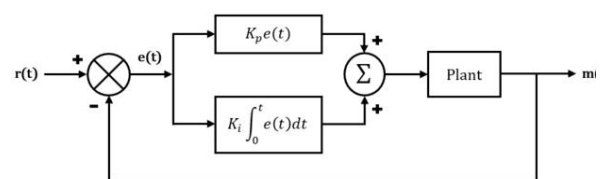


Figure 7. PI Controller Block Diagram

$$e(t) = r(t) - m(t) \quad (13)$$

E. Voltage Control Strategy

Figure 8 is the output voltage control strategy scheme proposed in this research.

Referring to Figure 8, $m(t)$ as V_{act} will be compared with $r(t)$ as V_{ref} resulting in $e(t)$, then processed using the PI control algorithm. The PI-controlled sinusoidal output signal (PI) will be compared with several control signals to produce SPWM and PWM switching signals.

1) For TP FBI

PI will be compared with 10 kHz carrier triangle waves that are mutually shifted by 180° to produce SPWM control signal for S1 and S3. PI will also be phase-shifted by 180° , resulting in $!PI$, and will be compared again with each carrier signal to produce SPWM control signal for S2 and S4. PI will be compared with Ground or 0 V as well, to produce 50 Hz PWM control signal for S5 and S6 (ZCD).

2) For TP AC-AC IBC

PI will be compared with Ground or 0 V to produce 50 Hz PWM control signal (Z). Then, Z will be fed to the OR logic gate circuits along with constant 10 kHz High-Frequency Pulse Width Modulation (HFPWM) signal, resulting in 10 kHz PWM control signal to operate Q1 – Q8.

The duty cycle of the switching signal is set first to 50%; the PI control will always compensate the value $e(t)$ so V_{act} will always adjust V_{ref} . Based on this description, it can be said that only the TP FBI section is controlled, while the PWM on the TP AC-AC IBC is constant, so that it can be called the independent control. The proposed control strategy flow is then simplified into a flowchart, as shown in Figure 9.

III. RESULTS AND DISCUSSION

A. Components and Parameters

TP IBI DC-AC circuit consists of 14 MOSFETs as power switches. The switching signals resulting from the processing of the STM32F406VET6 microcontroller are then fed to the driver circuit consisting of 14 TLP350 optocouplers as intermediaries for the

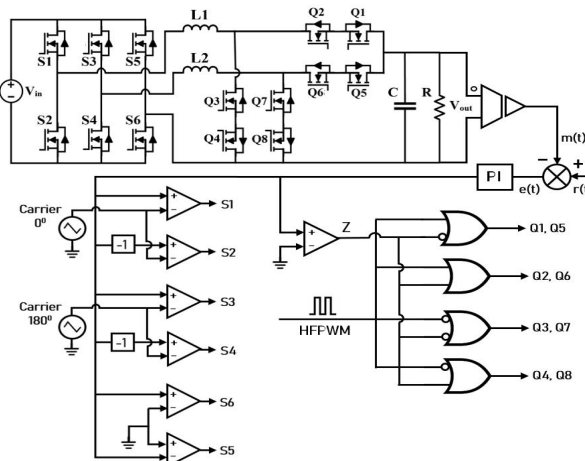


Figure 8. Proposed Control Voltage Strategy for TP DC-AC IBI

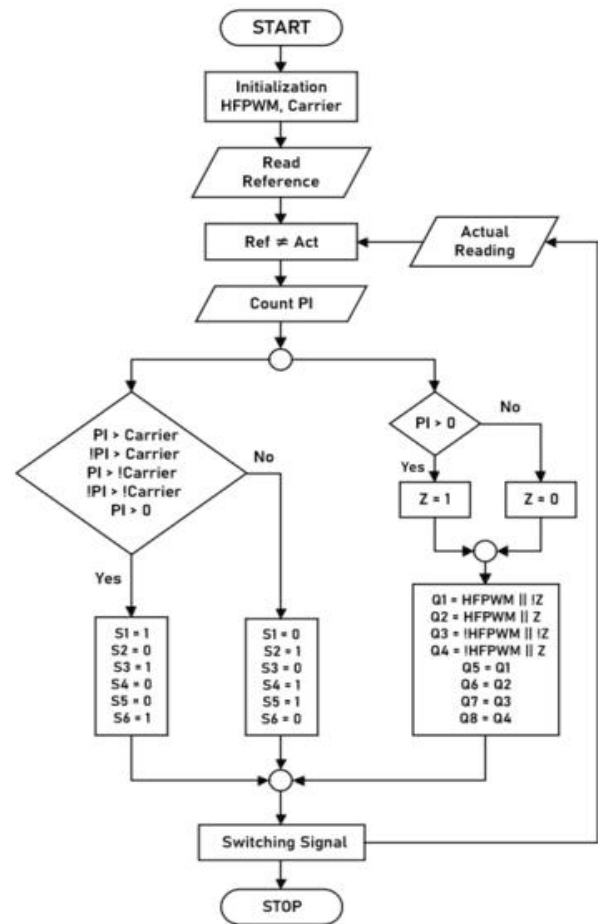


Figure 9. Flowchart of TP DC-AC Interleaved Boost Inverter Operation

switching signal at the gate of each MOSFET.

The computational simulation is then implemented in the laboratory hardware to prove the system that has been designed, with parameters as shown in Table 5. Figure 10 is a portrait of the implementation of the TP DC-AC IBI hardware in the laboratory, with component specifications as shown in Table 5.

B. Results and Discussion

The first four tests were carried out using a 10 Ω Resistor (R) as Load. The first test is the V_{in} and V_{out} test for TP DC-AC IBI. Figure 11(a) shows the relation between V_{in} and V_{out} , carried out by computational simulation with PSIM software. Figure 11(b) is the result of hardware testing measured using a Digital Oscilloscope (10x probes gain); using 50 VDC as V_{in} (blue), the TP DC-AC IBI is able to produce V_{out} (red)

TABLE 5
RESEARCH PARAMETERS

Components	Value
DC Input	50 VDC
Load Resistor R	5 Ω – 100 Ω
Capacitor C	47 μF
Inductors L1 & L2	2 mH
Switching Frequencies	10 kHz
Operational Frequency	50 Hz
Proportional Gain K_p	1
Integral Gain K_i	0.08

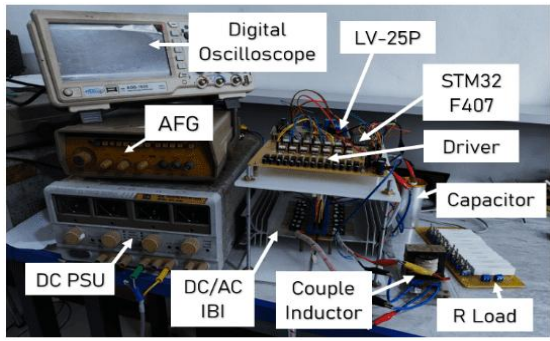
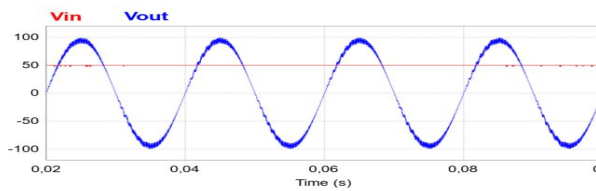


Figure 10. Hardware Laboratory Implementation

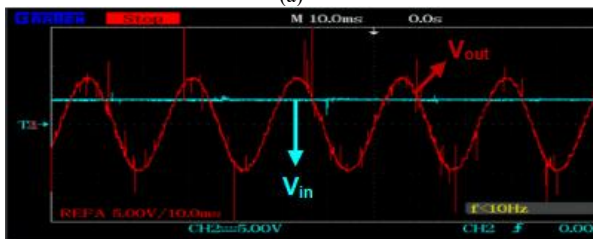
up to 100 VAC, which is almost twice the V_{in} , as shown in Figure 11(a). From the first test, it can be concluded that the TP DC-AC IBI in this research can work correctly as a voltage increaser and convert DC voltage to AC.

The second test was carried out using various test signals, namely sinusoidal, square and triangular waves which were carried out by simulation and computation. The actual voltage has been adjusted according to V_{ADC} which is 3.3 V at maximum. The second test uses LV-25P to prove whether V_{act} can always follow the desired V_{ref} . The first test signal used is a sinusoidal wave signal as V_{ref} with amplitude adjusted to 1.5 Vpp. Figure 12(a) shows the relation between V_{act} and V_{ref} in a computational simulation, here the two will always coincide (V_{act} always follow V_{ref}). Figure 12(b) shows the result of hardware measurements using a Digital Oscilloscope (1x probes gain); it can be seen that V_{act} (blue) always follows V_{ref} (yellow) as shown in the computational simulation result (Figure 12(a)).

The following tests use the triangular wave and square wave signal as V_{ref} using the same amplitude of 1.5 Vpp. Figures 13(a) and 14(a) show the relation between V_{act} and V_{ref} based on computational simulation, where the two will always coincide (V_{act} always follow V_{ref}). Figures 13(b) and 14(b) are the hardware measurement results using a Digital Oscilloscope; it can be seen that V_{act} (blue) always follows V_{ref} (yellow) as shown in computational

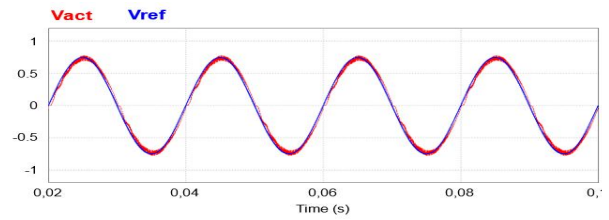


(a)

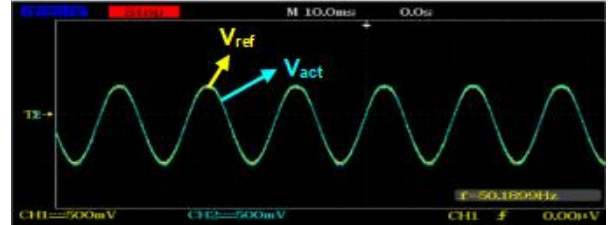


(b)

Figure 11. V_{in} and V_{out} measuring results using: (a) PSIM; and (b) Digital Oscilloscope

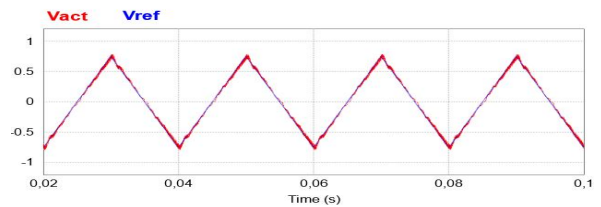


(a)

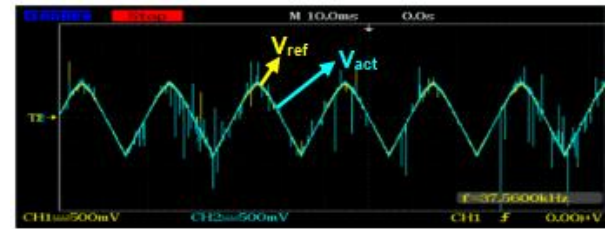


(b)

Figure 12. Sinusoidal Wave V_{ref} and V_{act} measuring results using: (a) PSIM; and (b) Digital Oscilloscope



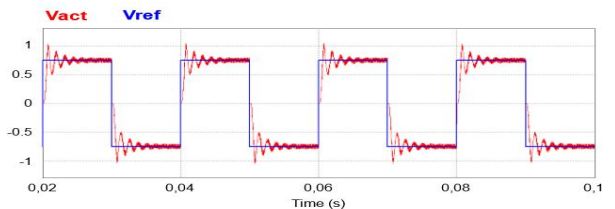
(a)



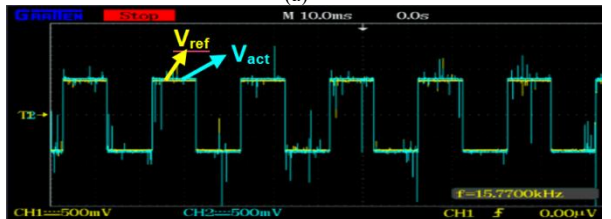
(b)

Figure 13. Triangular Wave V_{ref} and V_{act} measuring results using: (a) PSIM; and (b) Digital Oscilloscope

simulation (Figures 13(a) and 14(a)). Based on Figures 11 to Figure 14, it can be concluded that V_{act} can follow the desired V_{ref} value and even adjust the signal shape, which means the PI control applied to the TP DC-AC



(a)



(b)

Figure 14. Square Wave V_{ref} and V_{act} measuring results using: (a) PSIM; and (b) Digital Oscilloscope

IBI can always adequately compensate for the error signal, which means the controller works well.

The fourth test was carried out by comparing V_{out} with I_{out} . Figure 15(a) is the measurement result of V_{out} and I_{out} in computational simulation, where both are in phase (power factor ($\cos \varphi$) is unity). Figure 12(b) shows the result of hardware measurements using a Digital Oscilloscope, where V_{out} is measured at 100 VAC (10x probe gain), and I_{out} is approximately 1 A (1x probe gain); it can be seen that V_{out} (yellow) and I_{out} (blue) have identical shapes and are in phase, as shown in the computational simulation result (Figure 15(a)). This occurs because the system uses R as Load.

The final test is the Total Harmonic Distortion (THD) test for V_{out} and I_{out} , and also the system efficiency (η) test, using various R values. The load used is a resistor with a test value range from 5Ω to 100Ω . Thus, η can be determined by comparing the amount of power on the input (P_{in}) and output (P_{out}) sides, as shown at Equation (14).

$$\eta = \frac{P_{out}}{P_{in}} \times 100\% \quad (14)$$

Table 6 shows the P_{in} , P_{out} , η , and THD values obtained using various R values. Figure 16(a) shows the P_{out} versus η graph while Figure 16(b) shows the P_{out} versus THD graph. Both are based on Table 6, showing the P_{out} correlation between η and THD respectively.

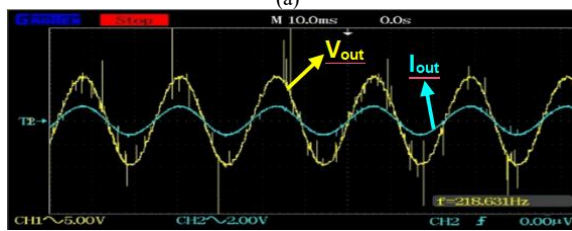
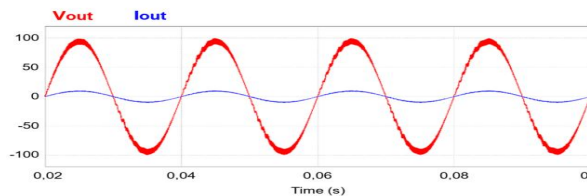


Figure 15. V_{out} and I_{out} measuring results using: (a) PSIM; and (b) Digital Oscilloscope

TABLE 6
OUTPUT POWER, EFFICIENCY, AND THD OBTAINED ON VARIOUS LOAD

R (Ω)	P_{in} (W)	P_{out} (W)	η (%)	THD (%)
5	943	797	84.51	5.88
10	489	441	90.18	3.56
20	241	217	90.04	3.29
30	151	137	90.72	3.27
40	126	115	91.26	3.09
50	96	89	92.71	3.13
60	82	76	92.68	2.84
70	71	66	92.96	2.71
80	65	60	92.30	2.49
90	58	54	93.10	2.53
100	49	46	93.87	2.46

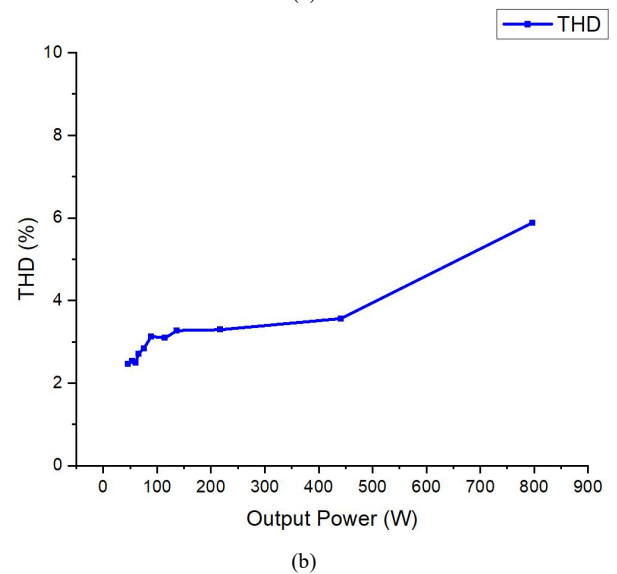
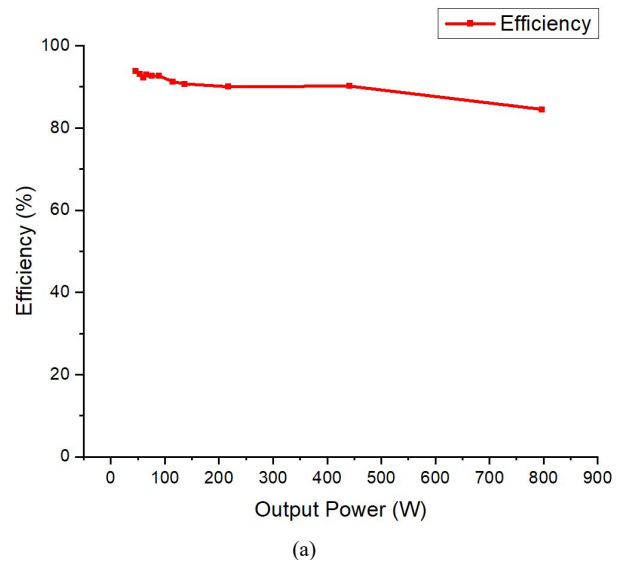


Figure 16. Output Power versus: (a) Efficiency; (b) THD; for various load values

We can conclude from Table 6 that the increase in P_{out} also causes THD to increase but decreases η . The small R value produces large i_{out} which resulting in a large P_{out} , and vice versa. Maximum P_{out} of 797 W is achieved using $R = 5 \Omega$, which resulting a minimum η at 84.51% and a maximum THD at 5.88%. While minimum P_{out} of 46 W is achieved using $R = 100 \Omega$, which resulting a maximum η at 93.87% and a minimum THD at 2.46%.

The THD obtained for V_{out} and I_{out} are both equal. According to the IEEE 519 standard, the THD value must not exceed 5%. Table 6 shows the THD results for the two in various R and P_{out} values. A 5.88% THD value is obtained, only when using R less than 10Ω , which is 5Ω . Using the other R values shown, the THD level meets the IEEE 519 Standard which is $< 5\%$.

IV. CONCLUSION

The TP DC-AC IBI prototype works correctly based on research and laboratory testing. Using 50 VDC as the input voltage, the proposed topology can generate an output voltage of up to 100 VAC, almost twice the input. The implemented PI control has been proven to regulate the system's output voltage so that it can constantly

adjust the reference's signal values and shapes. From the load changes test, it can be concluded that higher system power causes higher THD and lower efficiency. The system's efficiency is more than 90% on average, and meets the IEEE 519 THD Standard (2.46% - 3.56%) when using a 10 Ω Load value at a minimum. This TP DC-AC IBI has been proven to be able to produce high, regulated, less harmonic output and can be applied as an industrial-scale AC voltage provider utilizing RE sources such as wind turbines and PV panels.

DECLARATIONS

Conflict of Interest

The authors have declared that no competing interests exist.

CRediT Authorship Contribution

Juan Marco Alexander Wasiatno: Conceptualization, Methodology, Investigation, Data Curation, Software, Writing-Original Draft; Leonardus Heru Pratomo: Supervisor, Methodology, Data Curation, Resources, Validation, Writing-Reviewing & Editing.

Funding

Research reported in this publication was supported by Universitas Katolik (UNIKA) Soegijapranata Semarang and Matching Fund-Kedaireka Foundation (Directorate General of Higher Education, Research and Technology, Ministry of Education, Culture, Research and Technology Indonesia) under grant number: 23/E1/HK.02.02/2023 and No: 00387/H.3/Rek/04/2023.

Acknowledgment

The author would like to express gratitude to UNIKA Soegijapranata for supporting and preparing the equipment, instrumentations, electronical components and the laboratory for research and experimental purposes, Matching Fund-Kedaireka Foundation for funding and financial support, and Dr. Leonardus Heru Pratomo as the supervisor of the main contributor for the guidance and support during completion of this journal.

REFERENCES

- [1] K. S. Faraj and J. F. Hussein, "Analysis and comparison of dc-dc boost converter and interleaved dc-dc boost converter," *Eng. Technol. J.*, vol. 38, no. 5, pp. 622–635, May 2020, doi: 10.30684/etj.v38i5A.291.
- [2] A. V. Deshpande, B. K. Patil, R. B. Magadam, and N. R. Chitrakar, "Design and simulation of interleaved boost converter," *ICSCAN 2021*, no. July, pp. 1–5, 2021, doi: 10.1109/ICSCAN53069.2021.9526469.
- [3] K. . L. Shenoy, C. G. Nayak, and R. P. Mandi, "Design and implementation of interleaved boost converter," *Int. J. Eng. Technol.*, vol. 9, no. 3S, pp. 496–502, Jul. 2017, doi: 10.21817/ijet/2017/v9i3/170903S076.
- [4] Y. Y. Phyoo and T. L. Naing, "Modeling and simulation of two-phase interleaved boost converter using open-source software," *Int. J. Electr. Comput. Eng.*, vol. 12, no. 10, pp. 781–786, 2018.
- [5] R. Kumar, R. K. Singh, R. Kumar, and P. Mishra, "Design and simulation of interleaved boost converter," *Int. J. Res. Appl. Sci. Eng. Technol.*, vol. 11, no. 1, pp. 1760–1772, Jan. 2023, doi: 10.22214/ijraset.2023.48924.
- [6] G. V. B. Kumar and K. Palanisamy, "Interleaved boost converter for renewable energy application with energy storage system," *ICESIP 2019*, pp. 1–5, 2019, doi: 10.1109/ICESIP46348.2019.8938306.
- [7] B. A. Ikawanty and B. Irawan, "Four-phase interleaved boost converter for maximum power extraction in pv system," *Eduvest - J. Univ. Stud.*, vol. 3, no. 5, pp. 994–1006, 2023, doi: 10.59188/eduvest.v3i5.818.
- [8] S. N. Rao, S. K. Anisetty, B. M. Manjunatha, B. M. K. Kumar, V. P. Kumar, and S. Pranupa, "Interleaved high-gain boost converter powered by solar energy using hybrid-based mpp tracking technique," *Clean Energy*, vol. 6, no. 3, pp. 460–475, 2022, doi: 10.1093/ce/zkac026.
- [9] C. Abdelkhalik, E. B. Said, A. Younes, and A. Hassan, "A study and implementation of interleaved boost converter with a novel mppt tactic for pv systems," *ICECOCS 2020*, vol. 20, 2020, doi: 10.1109/ICECOCS50124.2020.9314470.
- [10] A. Ganesan and S. Kumaresan, "Transformerless high boost interleaved boost dc-dc converter for fuel cell application," *Aust. J. Basic Appl. Sci.*, vol. 10, no. 1, pp. 105–109, 2016.
- [11] S. M. Gopal and K. M. Reddy, "Design and control of high voltage gain interleaved boost converter for fuel cell based electric vehicle applications," *J. Electron., Comput. Netw. Appl. Math.*, vol. 3, no. 2, pp. 9–24, 2023, doi: 10.55529/jecnam.32.9.24.
- [12] R. Priya, R. Valli, and P. L. S. Krishnan, "Single stage dual boost inverter with half cycle modulation scheme for pv system applications," *ICSCAN*, pp. 1–8, 2019, doi: 10.1109/ICSCAN.2019.8878834.
- [13] M. F. Mohammed and M. A. Qasim, "Design dc / ac converter for renewable energy sources," *Int. J. Electr. Electron. Res. (IJEER)*, vol. 12, no. 2, pp. 682–687, 2024.
- [14] S. Phogat, "Analysis of single-phase spwm inverter," *Int. J. Sci. Res.*, vol. 3, no. 8, pp. 1793–1798, 2014.
- [15] R. Nagarajan, R. Yuvaraj, K. D. Kumar, R. D. Babu, M. Manikandan, and S. Meiyambu, "Implementation of spwm technique for inverter," *Int. J. of Adv. Res. Biol. Eng. Sci. Technol.*, vol. 2, no. 9, pp. 10–14, 2016.
- [16] P. Thasleena Mariyam, B. Paul, and K. Boby, "Transformerless inverter with interleaved boost converter for single phase pv systems," *SSRG Int. J. Electr. Electron. Eng.*, vol. 6, no. 5, pp. 44–48, 2019, doi: 10.14445/23488379/IJEEE-V6I5P108.
- [17] Z. B. Duranay and H. Guldemir, "Voltage controlled boost converter-inverter system for photovoltaic applications," *Turkish J. Sci. Technol.*, vol. 15, no. 2, pp. 85–92, 2020.
- [18] L. Pirashanthiyah, H. N. Edirisinghe, W. M. P. De Silva, S. R. A. Bolonne, V. Logeeshan, and C. Wanigasekara, "Design and analysis of a three-phase interleaved dc-dc boost converter with an energy storage system for a pv system," *Energies (Basel)*, vol. 17, no. 250, pp. 1–14, 2024, doi: 10.3390/en17010250.
- [19] S. Pillai and S. Thale, "Design and implementation of a three phase inverter for renewable energy source with unified control strategy," *Energy Procedia*, vol. 90, pp. 673–680, 2016, doi: 10.1016/j.egypro.2016.11.236.
- [20] L. Nguyen Quang and P. T. Nguyen, "Design and simulation of high-power dc-ac 3-phase inverter for island's power system using solar energy," *J. Technic. Edu. Sci. (JTE)*, no. 71A, pp. 8–17, 2022, doi: 10.54644/jte.71a.2022.1044.
- [21] Y. Koç, "Design of voltage transducer for digital signal processing development kit in implementation of a high step-up dc-dc converter," *J. Adv. Appl. Sci.*, vol. 2, no. 2, pp. 51–56, Dec. 2023, doi: 10.61326/jaasci.v2i2.99.
- [22] I. Laoprom and S. Tunyasirirut, "Design of pi controller for voltage controller of four-phase interleaved boost converter using particle swarm optimization," *J. Control Sci. Eng.*, vol. 2020, 2020, doi: 10.1155/2020/9515160.
- [23] R. K. Kadalgi and R. Dhanalakshmi, "Closed loop control of high voltage gain ibc with voltage multiplier module," *Int. J. Rec. Innov. Trends Comput. Commun.*, vol. 6, no. 5, pp. 165–170, 2018, doi: https://doi.org/10.17762/ijrctcc.v6i5.1597.
- [24] T. A. Odhafa, I. A. Abed, and A. A. Obed, "Controlling of boost converter by proportional integral controller," *Int. Trans. J. Eng. Manag. Appl. Sci. Technol.*, vol. 12, no. 4, pp. 1–8, 2021, doi: 10.14456/ITJEMAST.2021.66.
- [25] R. Nagarajan *et al.*, "Implementation of pi controller for boost converter in pv system," *Int. J. Adv. Res. Manag. Archit., Technol. Eng.*, vol. 2, no. 12, pp. 6–10, 2016, [Online]. Available: www.ijarmate.com.
- [26] M. H. Hariri, Mohamed, M. K. M. Desa, S. Masri, and M. A. A. M. Zainuri, "Design and implementation of three-phase voltage and current transducers for digital signal processing tms320f28335," *J. Electr. Syst.*, vol. 17, no. 1, pp. 141–153, 2021, doi: 10.6084/m9.figshare.14446074